Modelling of Electric Field Distributions on Cable Termination Defects under DC Plus Ripples

Shahtaj Shahtaj
Insitute for Energy and Environment
University of Strathclyde
Glasgow, United Kingdom
shahtaj@strath.ac.uk

Fulin Fan
Institute for Energy and Environment
Univeristy of Strathclyde
Glasgow, United Kingdom
f.fan@strath.ac.uk

Brian G. Stewart
Institute for Energy and Environment
University of Strathclyde
Glasgow, United Kingdom
brian.stewart.100@strath.ac.uk

***Abstract*—Cross-linked polyethylene (XLPE) cables are widely employed in high voltage transmission and medium voltage (MV) distribution networks due to the ease and low cost of forming the XLPE. However, defects in XLPE cable accessories such as joints and terminations will increase the local electric field and produce electrical discharges that erode the cable insulation and eventually result in the insulation failure. This paper develops finite element models to simulate small semicon tip defects at cable terminations and their resulting electric field distortion under MVDC stress voltage plus low frequency ripples. The influences of semicon tip lengths, ripple content and cable temperature gradients on electric field distributions are investigated to understand the electric field distortion surrounding semicon tip defects in relation to practical operation of MVDC XLPE cables.**

Keywords—Cross-linked polyethylene cable, electric field, finite element model, medium-voltage DC, ripple, semicon tip defect

I. Introduction

Medium-voltage (MV) DC networks have been considered one of the key technologies to facilitate the integration of distributed energy sources and accommodate electricity demand growth [1]. Most research related to MVDC focuses on the control and operation of power systems and converters [2]-[4], though less attention has been given to the influences of the transition to DC operation on MV power cables. In addition to the DC stress, DC cables are exposed to ripples coming from upstream AC systems or being generated by power converters [5]. As a consequence, it is necessary to understand the behaviour of MVDC cable insulation under different stresses for reliable operation.

Cross-linked polyethylene (XLPE) power cables are widely used in transmission and distribution networks [6] due to the high mechanical strength, chemical resistance and low dielectric losses of polyethylene insulation materials [7]. However, inadequate handling during cable manufacturing and installation can result in cable insulation defects [8], [9], including voids, corona, creepage, incision defects, metallic particles, semicon tips, axial direction shift defects and denting defects [10]. These defects may cause an increase in the local electric field and act as a source of discharges, accelerating the electrical breakdown and degradation of cable insulation [11].

The electric field distributions of DC cables with voids have been simulated in [12] and [13] to investigate the impacts of the void diameter and the distance of the void from the conductor on electric field distortion, respectively. Furthermore, the effects of air or water filled voids were examined in [14], finding that the electric field in air filled voids is more intense due to the smaller relative permittivity of air. The electric field distortion caused by different void defects was also compared in [15] by varying the void sizes, locations and shapes and filling the void with various materials such as air, water, fibre and copper. Other cable insulation defects including creepage, corona, scratch and cavity were simulated and verified by practical experiments in [16], showing that corona led to a high rate of discharges and the severest electric field distortion. In addition, the electric field distributions around air void, water film, metal debris and metal needle defects within cable samples were modelled by a charge-based simulation method and experimentally validated in [17], finding that the metal needle defect had the most intensive field compared to other defects under test.

The contribution of the paper is to evaluate the electric field distortion caused by small semicon tip defects of various lengths at XLPE cable terminations based on finite element models. In addition to a constant 11 kV DC stress, low frequency ripples at 300 Hz are applied to examine the effects of DC power quality issues on electric field distributions. Furthermore, the variation of electric field with cable temperature gradient across the cable is explored. The results will assist in understanding the electric field distortion in the case of semicon tip defects under practical operation of MVDC cables.

The paper is structured as follows. Section II describes the use of COMSOL Multiphysics for the simulation of XLPE cable termination with small semicon tip defects. Section III compares the electric field simulated with different semicon tip lengths, stress voltage profiles and cable temperature gradients. Conclusions and recommendations for further work are given in Section IV.

II. Methodology

The finite element method (FEM) is a numerical approach to calculating approximate solutions to different types of physical problems [18]. The XLPE cable termination geometry together with the semicon tip defects are simulated here by FEM in conjunction with COMSOL Multiphysics [19]. Fig. 1 shows the material, design and dimension of a 1-core 6.35/11kV MV cable modelled in 3D COMSOL. The cable has a solid aluminium

XXX-X-XXXX-XXXX-X/XX/$XX.00 ©20XX IEEE

This is a peer-reviewed, accepted author manuscript of the following paper: Shahtaj, S., Fan, F., & Stewart, B. (Accepted/In press). Modelling of electric field distributions on cable termination defects under DC plus ripples. In Proceedings of 2023 IEEE Electrical Insulation Conference (EIC) IEEE.

conductor and XLPE insulation, with a nominal cross section area of 185 mm^2. The cable consists of six layers, i.e., conductor, conductor screen, insulation, insulation screen, shielding wires and sheath. The considered layers are stripped out to form the cable termination for electric field simulation (see Fig. 1(b)). The semicon tip defect is assumed to occur at the left end of the insulation screen layer (i.e., outer semicon layer). Furthermore, the shape of the defect is presumed to be a rectangle with a semi-circle positioned at its end. While the tip width is fixed at 1 mm, its full length is set to 2 mm, 3 mm or 4 mm respectively to examine the effect of defect sizes. The relevant parameters of each cable layer are listed in Table I. Unlike AC cable, the insulation conductivity of DC cable is affected by the electric field and temperature. Higher conductor temperatures result in higher insulation conductivity near the conductor screen than near the insulation screen. As a result, the conductivity effect inverts the Laplacian field effect, increasing electric field stress near the insulation screen while decreasing it near the conductor screen. The electrical conductivity σ (S/m) of the insulation is formulated by (1) [22]:

$$\sigma(E,\vartheta) = D \cdot \exp(-B/(k_B \cdot \vartheta)) \cdot \exp\left(F \cdot \sqrt{E}/\vartheta\right) \quad (1)$$

where terms E and ϑ denote the electric field (kV/mm) and the temperature (K), respectively; coefficients D, B and F are equal to 659.5×10^{-3} (S/m), 0.85 (eV) and 150 ($K\sqrt{mm/kV}$), respectively; and the Boltzmann constant k_B equals 1.38065×10^{-23} in $J \cdot K^{-1}$.

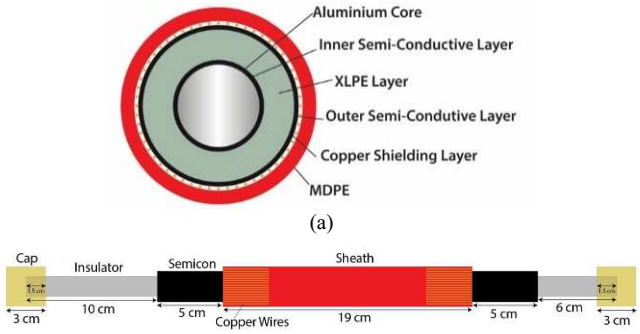

Fig. 1. (a) Top view and (b) side view of cable model.

TABLE I. MATERIAL PARAMETERS OF XLPE CABLE MODEL

Cable Layer	Relative Permittivity	Electrical Conductivity (S/m)
Conductor	1 [19]	3.774×10^7 [19]
Screen	1 [20]	1×10^{-4} [20]
Insulation	2.3 [21]	$\sigma(E,\vartheta)$ [22]
Shielding	1 [19]	5.998×10^7 [19]
Sheath	2.3 [23]	15.9×10^{-6} [23]

A pair of brass caps are mounted at the ends of the cable. The 11 kV DC voltage is injected through one of the caps, while the other cap models a termination and ensures symmetry of the cable model. Assuming the MVDC input to be supplied by a six-pulse converter, low frequency ripples at 300 Hz (given a 50 Hz nominal frequency on the AC side) with a magnitude of 4% of the nominal DC voltage [24] are additionally superimposed on the constant 11 kV stress to reflect the potential power quality in practice. As a comparison, the 300 Hz ripples with a magnitude equalling 10% of the nominal 11 kV are further tested. In addition, the sheath temperature is fixed at 20℃, while the core temperature is set to 20℃ and then 55℃ to examine the effect of temperature gradient inside the cable. The electric field of the cable is simulated by performing an electrostatic study under the COMSOL AC/DC module where the boundary condition for the interaction of two different media is formulated by (2).

$$\hat{n} \cdot (D_1 - D_2) = 0 \quad (2)$$

where $\hat{n}$ is the normal to the mathematical surface (or interface) pointing to the non-conducting region, and D_1 and D_2 denote the electric flux density vectors in the two media, respectively. The model is meshed by the physics-controlled mesh with fine element using quadratic elements.

III. RESULTS

The finite element model of the cable termination sample is implemented by COMSOL for different combinations of small semicon tip lengths, cable temperature gradients and ripple magnitudes. This section first discusses the influence of temperature gradient on the electric field of a non-defect cable sample, followed by comparing the field distortion induced by a semicon tip varying from 2 mm to 4 mm in length under 300 Hz ripples with a magnitude equalling 4% or 10% of the nominal 11 kV DC stress.

A. Impact of Temperature Gradient

The electric field distribution of a non-defect cable sample without any semicon tip defect is first simulated under 11 kV DC stress combined with zero and then 35ºC temperature gradient across the cable, as shown in Fig. 2. The electric field is shown to vary along the cable surface, with two significant peaks occurring at the junctions of the outer semicon layers due to the mismatch of relative permittivity between insulation and semicon layers. Furthermore, a higher peak is observed at the right junction which is closer to the brass cap. In addition, compared to the zero temperature gradient, the presence of the 35ºC temperature gradient increases the electric field peak from around 34 kV/cm to 51 kV/cm at the left junction and from around 58 kV/cm to 97 kV/cm at the right junction, indicating the necessity of modelling the temperature gradient caused by the Joule heating.

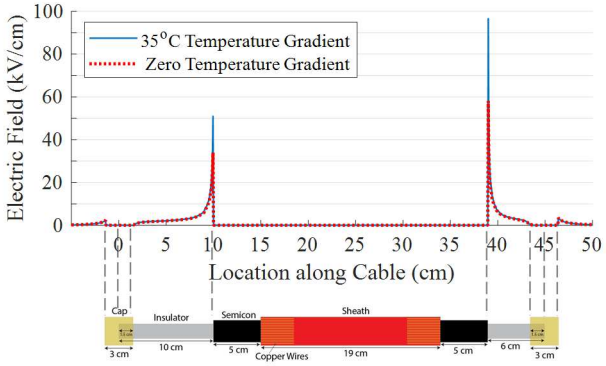

Fig. 2. The electric field (kV/cm) along the surface of a non-defect sample without defects under 11 kV DC stress and zero and 35℃ temperature gradient.

B. *Impact of Semicon Tip Defect Length*

The electric field distribution of the defective cable modelled with the three different semicon tip lengths under 11 kV DC stress and zero and 35ºC temperature gradient is shown in Figs. 3(a) and 3(b), where the semicon tip significantly increases the local electric field intensity to at least 600 kV/cm and 3,000 kV/cm respectively. This is because the sharp tip edge has a small area and thus a high potential gradient. Furthermore, the electric field intensity at the point of the tip generally increases with the tip length due to the reduced distance from the brass cap. Moreover, the field peaks generally occur at the front end (semi-circle) of the semicon tip, which can also be observed in the intensity map of the local electric field, as shown in Fig. 4. The findings obtained here for a symmetrical semicon tip defect could apply to arbitrary tip shapes, the electric field intensity around which would increase with their sharpness and length.

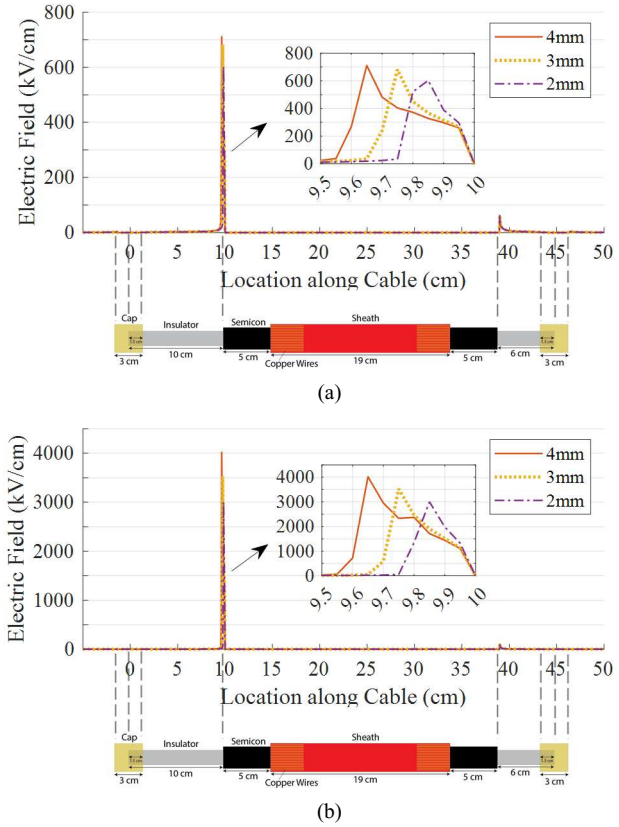

Fig. 3. The electric field (kV/cm) along the surface of a defective sample with the three different semicon tip lengths under 11 kV DC stress and (a) zero and (b) 35ºC temperature gradient.

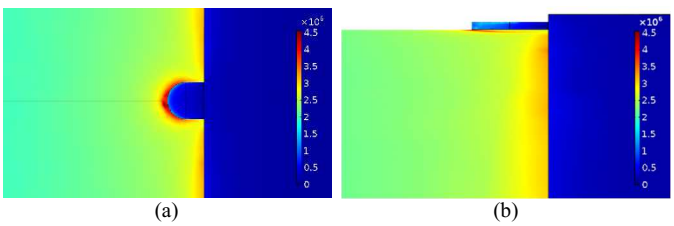

Fig. 4. The intensity maps of the local electric field (V/cm) (a) along the cable surface and (b) across the cut plane around a 2 mm semicon tip defect under 11 kV DC stress and 35ºC temperature gradient.

C. *Impact of DC Ripples*

Fig. 5 compares the electric field distortion simulated around the semicon tip between different ripple contents superimposed on the 11 kV DC stress under the two temperature gradients. The field distributions with the presence of 300 Hz ripples are very close to those that are simulated under constant DC voltage, showing a very slight increase in the field distortion. This illustrates that the ripples might be independent of the non-linear conductivity of cable insulation. However, the field distortion is shown to increase with the magnitude of the ripple. It can be seen that the intensity of the electric field increases with larger semicon tip size and also larger ripple. These results indicate that the electric field distribution will be further increased by greater ripples that might appear under fault and emergency conditions.

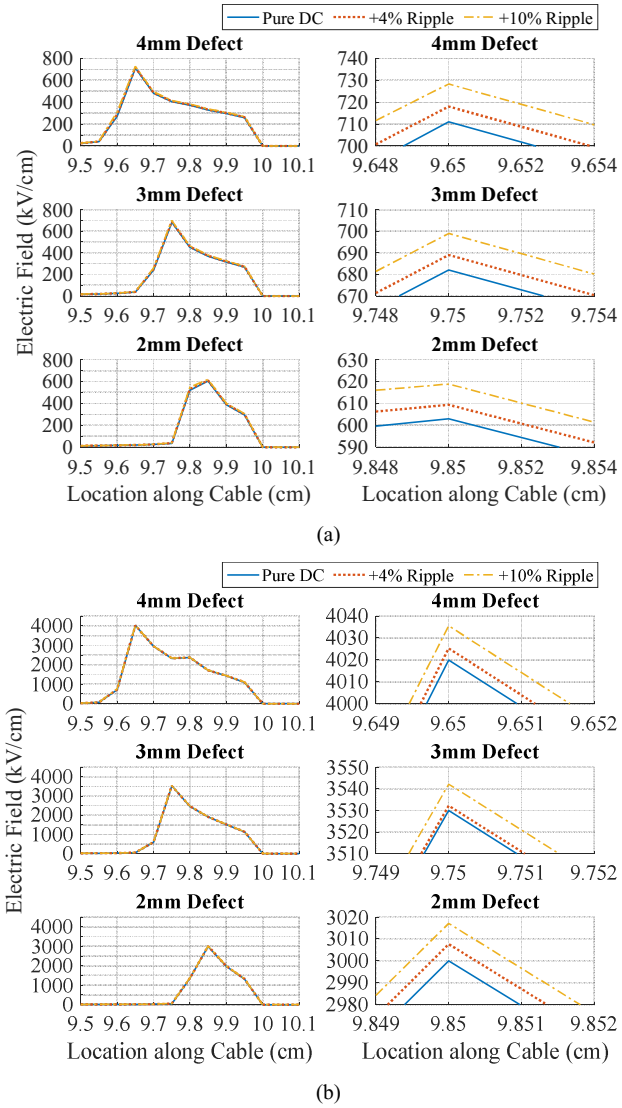

Fig. 5. The electric field (kV/cm) around the semicon tip defect with different tip lengths under (a) zero or (b) 35ºC temperature gradient and 11 kV DC stress with and without 300 Hz ripples (their enlarged graphs are listed on the right).

IV. Conclusions

The presence of defects at joints/terminations of cross-linked polyethylene (XLPE) cables can increase the local electric field intensity and reduce the insulation performance. To understand the electric field distortion induced by cable termination defects, this paper has developed finite element models to simulate the electric field distribution of a XLPE cable sample that is stripped out to form the cable termination under a medium-voltage (MV) DC stress of 11 kV. A small semicon tip defect in the shape of a rectangle linked with a semi-circle at its end is located at the boundary of the outer semicon layer. The width/diameter of the rectangle/semi-circle has been fixed at 1 mm, with the total tip length being altered between 2 mm and 4 mm to examine the variation of the resulting electric field distortion. Furthermore, the temperature gradient from the aluminium core to the cable sheath has been set to (55−20)℃ or (20−20)℃ to simulate the effect of the Joule heating created during operation. The simulation modelling has also included DC field inversion across the insulation based on Ref. Moreover, 300 Hz ripples with a magnitude of 4% or 10% of the nominal 11 kV have been additionally superimposed on the constant 11 kV stress to approximate the DC output voltage waveform more closely to potential practical stress levels.

The simulation results indicate that electric field peak occurring at the junction of the outer semicon layer increases with cable temperature gradient. Furthermore, the semicon tip defect significantly increases the local electric field compared to a non-defect cable sample due to the sharp tip edge having a high potential gradient. Moreover, the field distortion around the tip defect generally increases with the total tip length due to being closer to the brass cap where the voltage is injected. In addition, the electric field distortion increases with the magnitude of 300 Hz ripples, though the distortion increase due to the ripples is small, and dependent on the tip defect size.

Building on the present work, the finite element models will be extended to simulate the electric field distortion induced by different types and sizes of cable insulation defects. Furthermore, the field distortion increased by the ripple content under fault or emergency conditions will be examined. In addition, the defects simulated in the finite element models will be replicated on real cable samples for different tests such as partial discharge tests. This not only helps interpret the relationship of partial discharge patterns to DC power quality, but also permits correlating partial discharge patterns with insulation defect types to develop an innovative detection method for cable insulation defects.

Acknowledgment

The research was developed under the UK Engineering and Physical Sciences Research Council grant EP-T001445-1, and also a University of Strathclyde PhD Scholarship.

References

[1] J. Yu, K. Smith, M. Urizarbarrena, et al., “Initial designs for the ANGLE DC project: converting existing AC cable and overhead line into DC operation,” in *Proc. 13th IET Int. Conf. AC DC Power Transm.*, Manchester, UK, 2017, pp. 1-6.

[2] Y. Ji, Z. Yuan, J. Zhao, et al., “Hierarchical control strategy for MVDC distribution network under large disturbance,” *IET Gen. Transm. Distrib.*, vol. 12, no. 11, pp. 2557-2565, Jun. 2018.

[3] W. Liu, J. Yu, G. Li, et al., “Analysis and protection of converter-side AC faults in a cascaded converter-based MVDC link: ANGLE-DC project,” *IEEE Trans. Smart Grid*, vol. 13, no. 5, pp. 4046-4056, Sep. 2022.

[4] Q. Qi, C. Long, J. Wu, and J. Yu, “Impacts of a medium voltage direct current link on the performance of electrical distribution networks,” *Appl. Energy*, vol. 230, pp. 175-188, Nov. 2018.

[5] E. Corr, A. Reid, X. Hu, et al., “Partial discharge testing of defects in dielectric insulation under DC and voltage ripple conditions,” *CIGRE Sci. Eng.*, vol. 11, pp. 117-125, Jun. 2018.

[6] V. Vahedy, “Polymer insulated high voltage cables,” *IEEE Elect. Insul. Mag.*, vol. 22, no. 3, pp. 13-18, May-Jun. 2006.

[7] L.A. Dissado and J.C. Fothergill, Electrical Degradation and Breakdown in Polymers, 2nd Ed. Witlshire, London, UK: The Redwood Press, 1992, pp. 49-66.

[8] W. Vahlstrom, “Strategies for field testing medium voltage cables,” *IEEE Elect. Insul. Mag.*, vol. 25, no. 5, pp. 7-17, Sep.-Oct. 2009.

[9] H.E. Orton, “Diagnostic testing of in-situ power cables: an overview,” in *Proc. IEEE/PES Transm. Distrib. Conf. Exhib.*, Yokohama, Japan, 2002, pp. 1420-1425.

[10] Y. Jiang, H. Min, J. Luo, et al., “Partial discharge pattern characteristics of HV cable joints with typical aitificial defect,” in *Proc. 2010 Asia-Pacific Power Energy Eng. Conf.*, Chendu, China, pp. 1-4.

[11] T.G. Arachchige, L. Narampanawa, C. Ekanayake, and H. Ma, “Breakdown mechanisms of XLPE cable with insulation defects,” in *Proc. 95th IEEE Conf. Elect. Insul. Dielectric Phenomena*, East Rutherford, NJ, USA, 2020, pp. 71-74.

[12] U. Musa, A.A. Mati, A.A. Mas’ud, et al., “Modeling and analysis of electric field variation across insulation system of a MV power cable,” in *Proc. 3rd Int. Conf. Elect. Commun. Comput. Eng.*, Kuala Lumpur, Malasia, 2021, pp. 1-5.

[13] M.H.M. Sharif, N.A.M. Jamail, N.A. Othman, and M.S. Kamarudin, “Analysis of electric field and current density on XLPE insulator,” *Int. J. Elect. Comput. Eng.*, vol. 7, no. 6, pp. 3095-3104, Dec. 2017.

[14] C. Zhang and Z. Jia, “Electric field simulation of 10kV cable intermediate joint based on ingress defect,” in *Proc. 2021 Int. Conf. Elect. Mater. Power Equip.*, Chongqing, China, pp. 1-4.

[15] C.C. Uydur, O. Arikan, and O. Kalenderli, “The effect of insulation defects on electric field distribution of power cables,” in *Proc. 2018 IEEE Int. Conf. High Voltage Eng. Appl.*, Athens, Greece, pp. 1-4.

[16] Y. Zhu, F. Yang, X. Xie, et al., “Studies on electric field distribution and partial discharges of XLPE cable at DC voltage,” in *Proc. 12th IEEE Int. Conf. Properties Appl. Dielectric Mat.*, Xi’an, China, 2018, pp. 562-565.

[17] J. He, K. He, and L. Cui, “Charge-simulation-based electric field analysis and electrical tree propagation model with defects in 10 kV XLPE cable joint,” *Energies*, vol. 12, no. 23, p. 4519, Nov. 2019.

[18] K.-J. Bathe, “Finite element method,” in Wiley encyclopedia of computer science and engineering. New York: John Wiley & Sons, 2008.

[19] COSMOL Multiphysics. COMSOL, Inc., Stockholm, Sweden.

[20] Z. Nadolny, “Electric field distribution and dielectric losses in XLPE insulation and semiconductor screens of high-voltage cables,” *Energies*, vol. 15, no. 13, p. 4692, Jun. 2022.

[21] P.A. Ratheiser and U. Schichler, “Qualification of MVAC XLPE cables for DC operation,” in *Proc. 22nd Int. Symp. High Voltage Eng.*, Xi’an, China, 2021, pp. 1-6.

[22] P. Ratheiser and U. Schichler, “DC leakage current measurements: contribution for the qualification of extruded MVAC cables for DC operation,” in *Proc. 2021 IEEE Int. Conf. Properties Appl. Dielectric Mater.*, Johor Bahru, Malaysia, pp. 450-453.

[23] MatWeb, 31 Jan. 2023 last accessed, “Overview of Materials for Medium Density Polyethylene (MDPE), Extruded,” MatWeb. [Online]. Available: https://www.matweb.com/search/DataSheet.aspx?MatGUID=6aee274e12d64436afb46fa35d8bb07e&ckck=1

[24] *HVDC for Beginners and Beyond*, Alstom Grid, Paris, France, 2010.